TO APPEAR IN APJ LETTERS
Preprint typeset using LaTeX style emulateapj v. 5/2/11

IS IGR J11014–6103 A PULSAR WITH THE HIGHEST KNOWN KICK VELOCITY?

JOHN A. TOMSICK[1], ARASH BODAGHEE[1], JEROME RODRIGUEZ[2], SYLVAIN CHATY[2], FERNANDO CAMILO[3], FRANCESCA FORNASINI[1], & FARID RAHOUI[4,5]

To appear in ApJ Letters

ABSTRACT

We report on *Chandra* X-ray and Parkes radio observations of IGR J11014–6103, which is a possible pulsar wind nebula with a complex X-ray morphology and a likely radio counterpart. With the superb angular resolution of *Chandra*, we find evidence that a portion of the extended emission may be related to a bow shock due to the putative pulsar moving through the interstellar medium. The inferred direction of motion is consistent with IGR J11014–6103 having been born in the event that produced the supernova remnant (SNR) MSH 11–61A. If this association is correct, then previous constraints on the expansion of MSH 11–61A imply a transverse velocity for IGR J11014–6103 of 2,400–2,900 km s^{-1}, depending on the SNR model used. This would surpass the kick velocities of any known pulsars and rival or surpass the velocities of any compact objects that are associated with SNRs. While it is important to confirm the nature of the source, our radio pulsation search did not yield a detection.

Subject headings: stars: neutron — X-rays: stars — pulsars: general — ISM: supernova remnants — stars: individual (IGR J11014–6103, MSH 11–61A, SNR G290.1–00.8)

1. INTRODUCTION

IGR J11014–6103 was discovered as a hard X-ray (20–100 keV) source that was first seen during *INTEGRAL* (Winkler et al. 2003) observations of the Galactic Plane (Bird et al. 2010). Approximately 500 "IGR" sources[6] have been discovered or detected for the first time in hard X-rays by *INTEGRAL*. In the Galactic Plane, the *INTEGRAL* positions, which are typically accurate to a few arcminutes, are usually not sufficient to obtain source identifications. Thus, the field was followed-up with *Swift* observations, and a soft X-ray counterpart was detected (Malizia et al. 2011).

Pavan et al. (2011) report on *ROSAT*, *ASCA*, *Einstein*, *Swift*, and *XMM-Newton* observations of the region. While IGR J11014–6103 was the target for *Swift*, the other satellites observed the region in order to study the supernova remnant MSH 11–61A (SNR G290.1–00.8). From the X-ray observations, Pavan et al. (2011) find that IGR J11014–6103 has a complex X-ray morphology, consisting of a point source, an extended source that is $\sim$22″ North-East of the point source, and a streak of emission that extends to the North-West of the point source and is $\sim$4′ in length. Pavan et al. (2011) also search optical/IR, radio, and gamma-ray catalogs for counterparts, and they report a possible association with the radio source MGPS-2 J110149–610104, which has a flux of 24.2 ± 4.8 mJy at 843 MHz. They suggest that IGR J11014–6103 may be a pulsar wind nebula (PWN) produced by a high-velocity pulsar but conclude that X-ray observations with better angular resolution are required to establish the nature of the source.

Here, we report results of an observation with the *Chandra X-ray Observatory*, which provides the improved angular resolution.

2. *CHANDRA* OBSERVATION AND DATA REDUCTION

A *Chandra* observation of IGR J11014–6103 occurred on 2011 September 6 (ObsID 12420). We used the Advanced CCD Imaging Spectrometer (ACIS, Garmire et al. 2003) as the detector with the *INTEGRAL* position of IGR J11014–6103 at the ACIS-I aimpoint. The observation started at 1.43 hr UT, and a net exposure time of 4,991 s was obtained.

The data were initially processed at the *Chandra* X-ray Center (CXC) with ASCDS Version 8.4. After obtaining the data from the CXC, we performed all subsequent processing with the *Chandra* Interactive Analysis of Observations (CIAO) version 4.3.1 software and Calibration Data Base (CALDB) version 4.4.6. We used the CIAO program `chandra_repro` to produce the "level 2" event lists, which we analyzed as described below.

3. ANALYSIS AND RESULTS

An inspection of the 0.3–10 keV ACIS image indicates the presence of the complex source that was previously reported, and the point source (PS) and North-East (NE) extension are, by far, the brightest sources in the field-of-view. Figure 1 shows NE in far more detail than in previous observations, indicating that the emission may, in fact, have a conical or cometary shape with its narrow end close to PS.

3.1. *The Point Source*

We determined the *Chandra* position for PS using the CIAO routine `wavdetect`, and it is R.A. = $11^{\rm h}01^{\rm m}44^{\rm s}.96$, Decl. = –61°01′39″.6 (equinox 2000.0) with a 90% confidence uncertainty of 0″.64. Although the previously reported *XMM-Newton* position is marginally compatible with the $\sim$0″.1 (1-σ) near-IR position of 2MASS J11014532–6101383, the *Chandra* position is 3″.0 away, which rules out the association. Furthermore, we searched all of the source catalogs

[1] Space Sciences Laboratory, 7 Gauss Way, University of California, Berkeley, CA 94720-7450, USA (e-mail: jtomsick@ssl.berkeley.edu)
[2] AIM - Astrophysique Interactions Multi-échelles (UMR 7158 CEA/CNRS/Université Paris 7 Denis Diderot), CEA Saclay, DSM/IRFU/Service d'Astrophysique, Bât. 709, L'Orme des Merisiers, FR-91 191 Gif-sur-Yvette Cedex, France
[3] Columbia Astrophysics Laboratory, Columbia University, 550 West 120th Street, New York, NY 10027-6601, USA
[4] Harvard University, Astronomy Department, 60 Garden Street, Cambridge, MA 02138, USA
[5] Harvard-Smithsonian Center for Astrophysics, 60 Garden Street, Cambridge, MA 02138, USA
[6] See http://irfu.cea.fr/Sap/IGR-Sources.

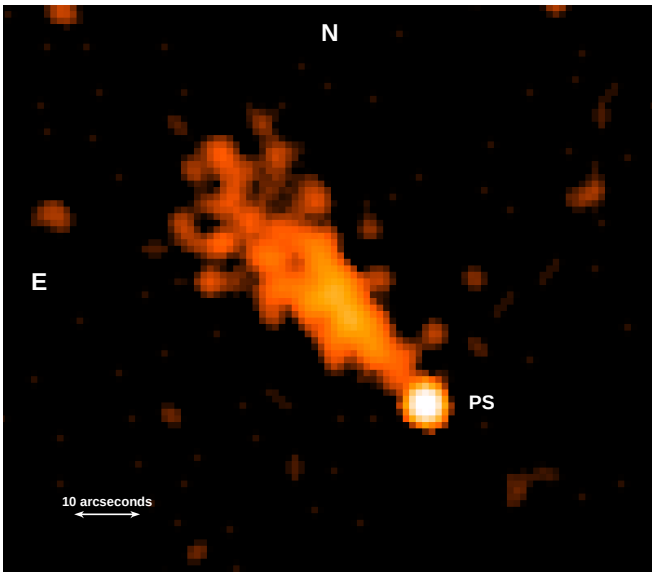

FIG. 1.— *Chandra*/ACIS 0.3–10 keV image of IGR J11014–6103. There is a point source (PS) and an extension to the North-East. The image has 0″.98 pixels and has been smoothed with a Gaussian kernel with a radius of 2″.95.

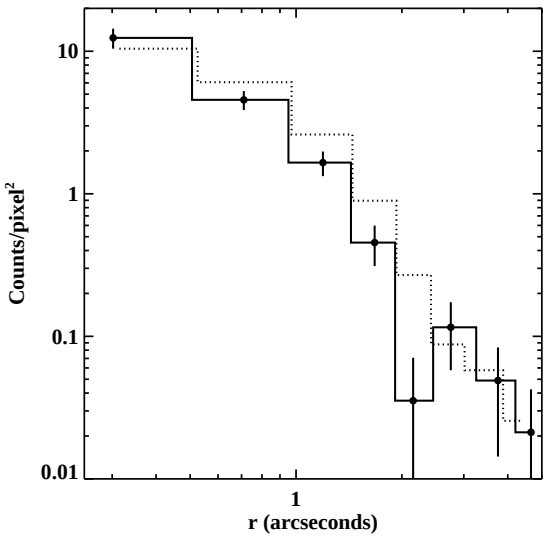

FIG. 2.— The radial profile of PS (*solid line*). The *dotted line* is the *Chandra* point spread function from "ChaRT" at the position of PS and with an energy spectrum like that of PS.

available in the VizieR database[7] with a search radius of 2″.0, and the *XMM-Newton* source is the only one that appears. Finally, we obtained near-IR images from 2MASS and optical images from the Digitized Sky Survey. Although there is no evidence for near-IR or optical sources at the *Chandra* position of PS, the nearby 2MASS source is relatively bright (J = 11.2, I = 13.0), making it difficult to obtain precise upper limits on the near-IR and optical brightnesses without higher quality images.

We also produced a radial profile for PS to determine if it is, in fact, a point source, and the profile is shown in Figure 2. We used *Chandra* Ray-Tracing software (ChaRT) and the *Chandra* simulator ("MARX") to calculate the point spread function (PSF) at the position of PS. The inputs to ChaRT were the off-axis angle (3′.64), the azimuth (330.82°), and the best fit spectrum for PS described below. Figure 2 shows that PS is consistent with being a point source. In fact, the simulated profile is slightly higher than the measurements for PS, and this is likely due to inaccuracies within ChaRT or MARX as has also been found by Bogdanov et al. (2011).

We extracted an energy spectrum for PS using the CIAO program `specextract`. We used an aperture with a radius of 5″ for the source spectrum, and a nearby rectangular source-free region for the background spectrum. We extracted 126 counts in the source region in the 0.3–10 keV band, and the background estimate (scaled to the size of the source region) is 0.8 counts. We fitted the energy spectrum using the XSPEC software package. A model consisting of a power-law with interstellar absorption provides a good description of the spectrum. The power-law photon index is $\Gamma = 1.5^{+0.6}_{-0.5}$ (90% confidence uncertainties are given here and below), and the unabsorbed 0.3–10 keV flux is $(8.6^{+3.6}_{-1.7}) \times 10^{-13}$ erg cm^{-2} s^{-1}. Using Wilms, Allen & McCray (2000) abundances and Balucinska-Church & McCammon (1992) cross sections, we obtained a column density of $N_{\rm H} = (1.6^{+0.9}_{-1.1}) \times 10^{22}$ cm^{-2}. This is consistent with the previous value measured with *XMM-Newton* (Pavan et al. 2011).

We also checked for long and short-term variability of PS. Using the spectral shape described above, the *Chandra* observation indicates an absorbed 2–10 keV flux of 5.5×10^{-13} erg cm^{-2} s^{-1}, and the flux obtained in the same band using the *XMM-Newton* observation is $(6.2^{+0.9}_{-2.6}) \times 10^{-13}$ erg cm^{-2} s^{-1} (Pavan et al. 2011). Thus, there is no evidence for flux variations between the 2003 and 2011 observations. Using *XMM-Newton*, Pavan et al. (2011) find no indication of variability on time scales of seconds to hours. We searched for variability with *Chandra* down to a time scale of 50 s using the CIAO tool `glvary` (Gregory & Loredo 1992) and did not detect variations.

3.2. *The North-East Extension*

We extracted an energy spectrum for NE from a 24″-by-46″ rectangular region rotated to a position angle of 45°. We chose the region to include all of the counts from NE and to exclude the counts from PS. We extracted 261 counts in the source region in the 0.3–10 keV band, and the background estimate (scaled to the size of the source region) is 11.7 counts. A model consisting of a power-law with interstellar absorption provides a good description of the spectrum. The power-law photon index is $\Gamma = 1.8 \pm 0.4$ and the column density is $N_{\rm H} = (0.8^{+0.4}_{-0.3}) \times 10^{22}$ cm^{-2}. The unabsorbed 0.3–10 keV flux is $(1.3^{+0.4}_{-0.2}) \times 10^{-12}$ erg cm^{-2} s^{-1}. The spectral parameters are consistent with those found by Pavan et al. (2011), but the flux measured by *Chandra* (the absorbed 2–10 keV flux is 6.4×10^{-13} erg cm^{-2} s^{-1}) is a factor of ∼1.7 higher. It is possible that this difference reflects a true change in flux, but it may also be related to the fact that PS and NE are not fully resolved by *XMM-Newton*.

Profiles of detected counts for PS and NE are shown in Figure 3a. We extracted counts from a 24″-by-80″ rectangular region rotated at a position angle of 45° that includes both PS and NE. We produced profiles of the counts along the long axis of the rectangle in two energy bands, 0.3–10 keV and 2–10 keV. While the number of 2–10 keV counts is close to half the number in the full energy band, the profiles are not significantly different. The profile for NE peaks between 15″ and 30″ from PS.

[7] See http://webviz.u-strasbg.fr/viz-bin/VizieR-4.

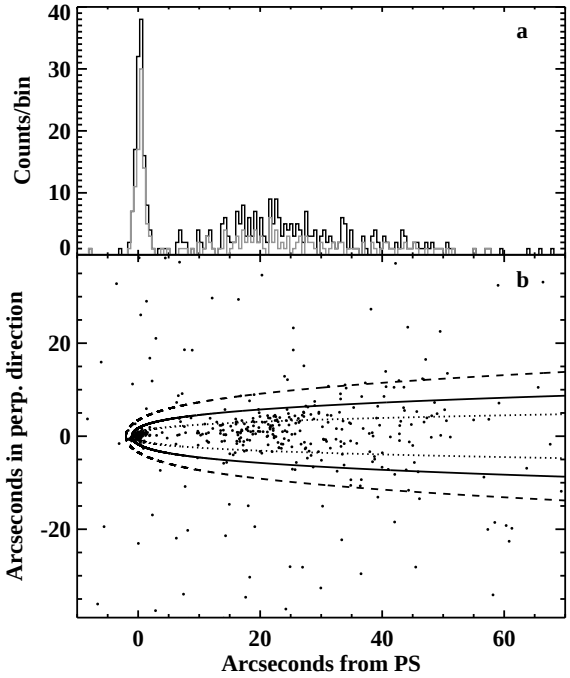

FIG. 3.— *(a)* Counts profiles for PS and NE in two energy bands: the full 0.3–10 keV band (black) and the 2–10 keV band (grey). The horizontal axis runs through PS and NE at a position angle of 45°, and the counts in the perpendicular direction within $\pm 12''$ of the axis are summed. *(b)* Unbinned 0.3–10 keV image where each dot corresponds to the location of an X-ray detection. The dotted, solid, and dashed lines represent the predicted locations of the bow shock for $\delta_{SO} = 0''.4$, $1''$, and $2''$, respectively, assuming $i = 0°$.

3.3. *The X-ray Tail*

In addition to PS and NE, the X-ray "tail" that was previously reported from the *XMM-Newton* observations in Pavan et al. (2011) is also detected (see Figure 4). The length of the tail is several arcminutes, and it is nearly perpendicular to the NE extension.

4. RADIO PULSAR SEARCH

We searched for pulsations from IGR J11014–6103 on 2011 July 27 using the CSIRO Parkes radio telescope. We obtained a 5.6 hr observation with the 1.4 GHz multibeam receiver and sampled every 1 ms each of the 96 frequency channels spanning 288 MHz of bandwidth (for further data acquisition details, see Manchester et al. 2001). We analyzed the data following standard pulsar search techniques using PRESTO (Ransom 2001), but did not identify a convincing pulsar candidate. We dedispersed the data up to DM = 1280 pc cm^{-3}, which is twice the maximum predicted in this direction by the Cordes & Lazio (2002) model for the Galactic distribution of free electrons. The sensitivity limit of this observation, assuming a pulsar duty cycle of 10%, is $S_{1.4}$ = 0.05 mJy, corresponding to a luminosity ($L_{1.4} \equiv S_{1.4}d^2$) limit of $<$0.05 mJy kpc^2 at a distance of 1 kpc and $<$5 mJy kpc^2 at d = 10 kpc. If the source is at the larger distance, the non-detection is not surprising since approximately half of all young pulsars detected in the radio have luminosities below 5 mJy kpc^2 (see Camilo et al. 2009).

5. DISCUSSION

The results presented above are consistent with (but do not prove) the hypothesis that PS is a pulsar. The *Chandra* position shows that the source does not have a bright optical/IR counterpart, which is consistent with a pulsar since isolated neutron stars are very faint in the optical and IR. The stability of the long-term flux and the power-law spectrum are also expected if the source is a pulsar.

The *Chandra* observation provides new information about the NE extension and its relationship to PS. In the scenario where PS is a pulsar, the natural explanation for NE is that it is a PWN as suggested by Pavan et al. (2011). For some PWNe, a bow shock is created due to the motion of the pulsar through the ISM. In the case of IGR J11014–6103, the morphology of NE suggests that the pulsar may be moving in the South-West direction at high speed. Figure 4 provides evidence in favor of this interpretation as it shows that NE is elongated in a direction that is co-aligned with PS and the center of the SNR MSH 11–61A. Thus, a strong possibility is that the compact object that is powering IGR J11014–6103 was produced when the supernova occurred.

MSH 11–61A has a centrally bright X-ray morphology, but the location of the compact object produced in the supernova is unknown. The X-ray emission from the SNR is thermal rather than being powered by a PWN (Slane et al. 2002). It has been suggested that PSR J1105–6107, which is $22'$ from the center of the SNR, may be associated with MSH 11–61A (Kaspi et al. 1997). Applying SNR evolution models to MSH 11–61A, Slane et al. (2002) argue that the SNR is (1–2)$\times 10^4$ yr old and is at a distance of 8–11 kpc. The thermal conduction and cloudy ISM models would imply transverse velocities for PSR J1105–6107 of 4,500 and 5,300 km s^{-1}, respectively (Slane et al. 2002). In contrast, the known distribution of pulsar velocities includes groups near 175 km s^{-1} and 700 km s^{-1} (Cordes & Chernoff 1998). The fastest pulsar with parallax and proper motion measurements has a velocity of 1,100 km s^{-1} (Chatterjee et al. 2005). Although there is evidence for pulsar or compact object velocities in excess of 1,100 km s^{-1} (Hui & Becker 2006; Winkler & Petre 2007), $>$1,000 km s^{-1} (Ng et al. 2011), and $>$1,400 km s^{-1} (Lovchinsky et al. 2011), the velocities implied by an association between PSR J1105–6107 and MSH 11–61A are likely too high.

IGR J11014–6103 is $11'.9$ from the center of MSH 11–61A, and scaling from the calculations previously carried out for PSR J1105–6107, we determine transverse velocities of 2,400 and 2,900 km s^{-1} for the thermal conduction and cloudy ISM models, respectively, if IGR J11014–6103 was formed in the supernova event that produced MSH 11–61A. Among known compact objects associated with SNRs, these values are only rivaled by the recent estimate of 1,400–2,600 km s^{-1} for XMMU J172054.5–372652 (Lovchinsky et al. 2011). Thus, these two cases indicate that supernova models that can produce $>$2,000 km s^{-1} kick velocities may be required.

5.1. *The PWN Bow Shock Interpretation and Implications*

If the interpretation that IGR J11014–6103 is a PWN and that NE is emission from a bow shock is correct, then the fact that PS is a point source along with the morphology of NE provide a constraint on the angular distance between the pulsar and the standoff shock, $\delta_{SO} = R_{SO} \cos i/d$, where R_{SO} is the standoff shock radius, i is the inclination angle of the pulsar velocity with respect to the plane of the sky, and d is the distance to the source. The standoff shock location is set by the ram pressure balance between the pulsar wind and the pulsar passing through the interstellar medium (ISM). The shape of

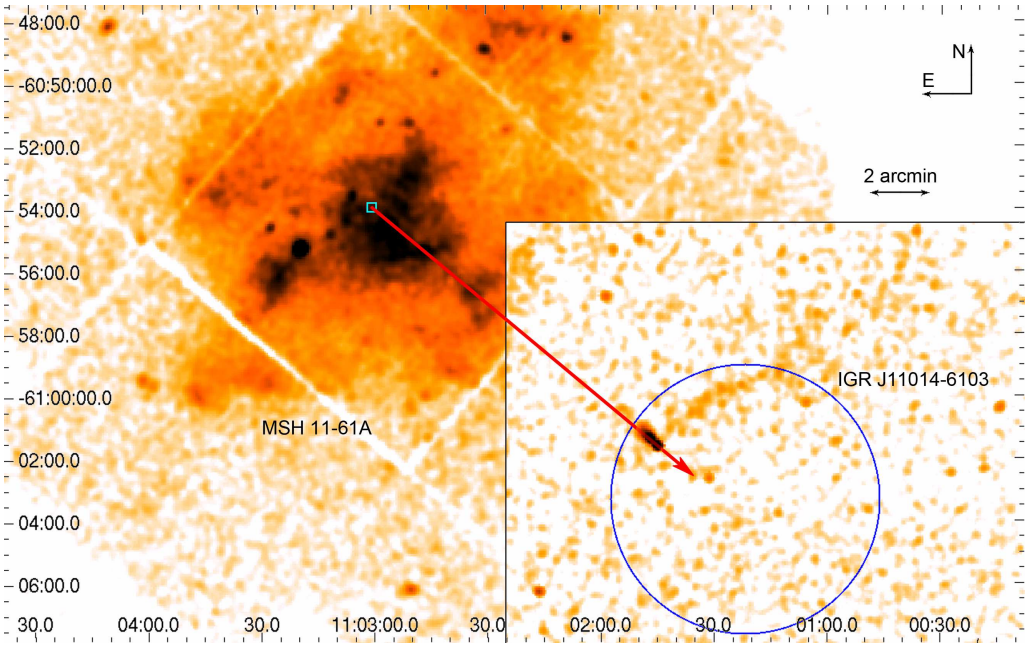

FIG. 4.— Composite image of the supernova remnant MSH 11–61A near IGR J11014–6103. The large image is from *XMM-Newton* (0.5–10 keV), while the inset is from *Chandra*-ACIS (0.3–10 keV): both were rebinned and smoothed. The blue circle is the 4′.3 *INTEGRAL* error circle. It is shown via the red arrow that sources PS, NE, and the center of the SNR, marked with a cyan square, are co-aligned. The 4′ X-ray tail to the North-West of PS can also be seen.

the entire bow shock in space is determined by $R_{\rm SO}$ according to

$$R(\phi) = \frac{R_{\rm SO}}{\sin\phi}\sqrt{3(1-\frac{\phi}{\tan\phi})} \quad , \qquad (1)$$

where ϕ is the angle with respect to the direction of motion, and R is the distance to the shock along each angle (Wilkin 2000). While the observed shape of the bow shock will depend on i, here, we make a rough estimate for $\delta_{\rm SO}$ using the $i = 0°$ case. Figure 3b compares the calculated shape of the bow shock to the *Chandra* data for three values of $\delta_{\rm SO}$. The data are best described by a value close to 1″, and the lower and upper limits are approximately 0″.4 and 2″, respectively.

Following Caraveo et al. (2003), we derive

$$\delta_{\rm SO} = 0''.266\frac{\cos^2 i}{v_{t,3}\, d_{10}}(\frac{\dot{E_{36}}}{n_{0.1}})^{1/2} \quad , \qquad (2)$$

where $v_{t,3}$ is the transverse velocity of the pulsar in units of 10^3 km s^{-1}, d_{10} is the distance to the pulsar in units of 10 kpc, $\dot{E_{36}}$ is the rotational energy loss of the pulsar in units of 10^{36} erg s^{-1}, and $n_{0.1}$ is the particle density of the ISM near the source in units of 0.1 cm^{-3}.

From the spectral fits described above, the 0.3–10 keV unabsorbed flux of PS and NE combined is 2.2×10^{-12} erg cm^{-2} s^{-1}, which corresponds to a luminosity of $2.6 \times 10^{34}\ d_{10}^2$ erg s^{-1}, and as η is the radiative efficiency of the PWN, $\dot{E_{36}} = 0.026 d_{10}^2 \eta^{-1}$. We obtain another constraint by considering that if NE is a PWN, then the emission has a synchrotron origin and will decay as the electrons age on a time scale of $t_{s,3}$, where this is the exponential e-folding time for the X-ray flux in units of 10^3 yr. Thus, the ∼1′ transverse length of NE implies that $v_{t,3} = 2.8 d_{10} t_{s,3}^{-1}$, and the expression for the standoff shock radius becomes

$$\delta_{\rm SO} = 0''.015\frac{\cos^2 i\, t_{s,3}}{d_{10}\, n_{0.1}^{1/2}\, \eta^{1/2}} \quad . \qquad (3)$$

A significant caveat is that the synchrotron lifetime constraint assumes that any velocity imparted to electrons in the PWN by the pulsar is small relative to the pulsar space velocity. If NE has a magnetotail component (Romanova, Chulsky & Lovelace 2005), then the ejection velocities could be high enough to invalidate this assumption (Kargaltsev et al. 2008).

Figure 5 shows the distance-$\delta_{\rm SO}$ parameter space for the case of $i = 0°$, $t_{s,3} = 1$, and $n_{0.1} = 1$ for several different values of η that span values measured for ∼60 PWN (Kargaltsev & Pavlov 2010). The value of $t_{s,3} = 1$ is obtained in the Caraveo et al. (2003) study, and it is what would be predicted for a ∼10 μG magnetic field (Kargaltsev et al. 2008). The value of $n_{0.1} = 1$ is consistent with the intercloud ISM density found in the vicinity of MSH 11–61A using the cloudy ISM model (Slane et al. 2002). The *Chandra* constraints on $\delta_{\rm SO}$ suggest a value of $\eta \sim 10^{-2}$ if the distance is ∼2 kpc and values of $\eta \sim 10^{-3}$–10^{-4} if the distance is ∼10 kpc. Although we cannot use this information to formally constrain the distance, the larger distance is slightly favored since PWNe with $\eta = 10^{-3}$–10^{-5} are much more common than PWNe with larger radiative efficiencies (Kargaltsev & Pavlov 2010).

5.2. *X-ray Tails from PWNe*

Whether IGR J11014–6103 is related to MSH 11–61A or not, if PS is a pulsar moving in a South-West direction as implied by NE being a bow shock, then the X-ray tail extends ∼4′ in a direction that is ∼perpendicular to the motion of the pulsar. A chance alignment seems unlikely, especially since similar X-ray tails have been seen from other PWNe. Examples include the Guitar Nebula

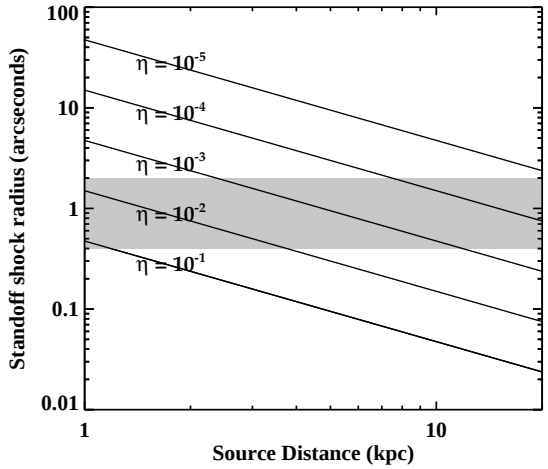

FIG. 5.— Parameter space for the distance to IGR J11014–6103 and the standoff shock radius (δ_{SO}), if NE is indeed a bow shock. From the *Chandra* image, we find that values of δ_{SO} between 0″.4 and 2″.0 are allowed (for $i = 0°$). The solid lines show the calculated values for a range of pulsar efficiencies (η) for the case where $i = 0°$, $n_{0.1} = 1$, and $t_{s,3} = 1$.

(PSR B2224+65) and PSR J0357+3205, which have 2′ and 9′ X-ray tails (Hui & Becker 2007; De Luca et al. 2011). The Guitar Nebula is noteworthy because its X-ray tail points in a direction that is 118° from the measured proper motion direction for this pulsar (Hui & Becker 2007; Hui et al. 2011).

While these examples support the PWN nature of IGR J11014–6103 as discussed by Pavan et al. (2011) and also the possibility that the IGR J11014–6103 X-ray tail may extend in a direction perpendicular to the pulsar's direction of motion, it is worth pointing out that the size of the X-ray tail may be an argument against a ∼10 kpc distance. While the X-ray tails for the other pulsars have lengths near 1 pc, a 10 kpc distance for IGR J11014–6103 would imply a ∼10 pc length for the X-ray tail from this source.

6. SUMMARY AND CONCLUSIONS

This work provides further evidence that IGR J11014–6103 is a PWN. The *Chandra* position for PS eliminates the previously suggested 2MASS counterpart, and the available near-IR and optical images do not indicate the presence of another counterpart, which is consistent with the faint levels of optical/IR emission expected from a pulsar. Most significantly, the *Chandra* observation has provided new information about the morphology of the extended source to the North-East of PS (called NE in this work), and we argue that the most likely interpretation is that NE is shaped by a bow shock caused by PS moving in the South-West direction at a high rate of speed.

Given the alignment of PS, NE, and the supernova remnant MSH 11–61A, we suggest the possibility that IGR J11014–6103 is a pulsar that was formed by the supernova event that produced MSH 11–61A. If correct, this would imply that IGR J11014–6103 is at the same distance as the SNR, 8–11 kpc, and also that the supernova imparted a kick velocity of at least 2,400–2,900 km s^{-1}. While we show that the *Chandra* constraint on the standoff shock makes a scenario with a large distance and a high velocity plausible, caution is required due to uncertainties about the nature of the source, its orientation in space (i), and its environment. One possible counterargument to IGR J11014–6103 having a distance compatible with the SNR is that this would imply a 10 pc-long X-ray tail.

We acknowledge useful discussions with J. Halpern, V. Kaspi, and S. Boggs. Support for this work was provided by NASA through *Chandra* Award Number GO1-12046X issued by the *Chandra* X-ray Observatory Center, which is operated by the Smithsonian Astrophysical Observatory under NASA contract NAS8-03060. The Parkes Observatory is part of the Australia Telescope, which is funded by the Commonwealth of Australia for operation as a National Facility managed by CSIRO.

REFERENCES

Balucinska-Church, M., & McCammon, D., 1992, ApJ, 400, 699
Bird, A. J., et al., 2010, ApJS, 186, 1
Bogdanov, S., Archibald, A. M., Hessels, J. W. T., Kaspi, V. M., Lorimer, D., McLaughlin, M. A., Ransom, S. M., & Stairs, I. H., 2011, ApJ, 742, 97
Camilo, F., Ng, C.-Y., Gaensler, B. M., Ransom, S. M., Chatterjee, S., Reynolds, J., & Sarkissian, J., 2009, ApJ, 703, L55
Caraveo, P. A., Bignami, G. F., De Luca, A., Mereghetti, S., Pellizzoni, A., Mignani, R., Tur, A., & Becker, W., 2003, Science, 301, 1345
Chatterjee, S., et al., 2005, ApJ, 630, L61
Cordes, J. M., & Chernoff, D. F., 1998, ApJ, 505, 315
Cordes, J. M., & Lazio, T. J. W., 2002, arXiv:astro-ph/0207156
De Luca, A., et al., 2011, ApJ, 733, 104
Garmire, G. P., Bautz, M. W., Ford, P. G., Nousek, J. A., & Ricker, G. R., 2003, in X-Ray and Gamma-Ray Telescopes and Instruments for Astronomy. Edited by Joachim E. Truemper, Harvey D. Tananbaum. Proceedings of the SPIE, 4851, 28
Gregory, P. C., & Loredo, T. J., 1992, ApJ, 398, 146
Hui, C. Y., & Becker, W., 2006, A&A, 457, L33
Hui, C. Y., & Becker, W., 2007, A&A, 467, 1209
Hui, C. Y., Huang, R. H. H., Trepl, L., Tetzlaff, N., Takata, J., Wu, E. M. H., & Cheng, K. S., 2011, arXiv:1112.5816
Kargaltsev, O., Misanovic, Z., Pavlov, G. G., Wong, J. A., & Garmire, G. P., 2008, ApJ, 684, 542
Kargaltsev, O., & Pavlov, G. G., 2010, X-ray Astronomy 2009; Present Status, Multi-Wavelength Approach and Future Perspectives, 1248, 25
Kaspi, V. M., Bailes, M., Manchester, R. N., Stappers, B. W., Sandhu, J. S., Navarro, J., & D'Amico, N., 1997, ApJ, 485, 820
Lovchinsky, I., Slane, P., Gaensler, B. M., Hughes, J. P., Ng, C.-Y., Lazendic, J. S., Gelfand, J. D., & Brogan, C. L., 2011, ApJ, 731, 70
Malizia, A., Landi, R., Bassani, L., Bird, A. B. A. J., Gehrels, N., & Kennea, J. A., 2011, The Astronomer's Telegram, 3290
Manchester, R. N., et al., 2001, MNRAS, 328, 17
Ng, C.-Y., Bucciantini, N., Gaensler, B. M., Camilo, F., Chatterjee, S., & Bouchard, A., 2011, arXiv:1109.2233
Pavan, L., Bozzo, E., Pühlhofer, G., Ferrigno, C., Balbo, M., & Walter, R., 2011, A&A, 533, A74
Ransom, S. M., 2001, *Ph.D. thesis*, Harvard University
Romanova, M. M., Chulsky, G. A., & Lovelace, R. V. E., 2005, ApJ, 630, 1020
Slane, P., Smith, R. K., Hughes, J. P., & Petre, R., 2002, ApJ, 564, 284
Wilkin, F. P., 2000, ApJ, 532, 400
Wilms, J., Allen, A., & McCray, R., 2000, ApJ, 542, 914
Winkler, C., et al., 2003, A&A, 411, L1
Winkler, P. F., & Petre, R., 2007, ApJ, 670, 635